(slope of % occurrence of muscle SNA burst over 1 mmHg binned AP, eliminating strength of SNA burst) correlated with it mildly ($r^2 = 0.5$). Although we cannot directly compare the transfer function analysis in our present study with the spontaneous threshold measure reported by Hart *et al.* (2010) because of methodological differences, our open-loop transfer function of the neural arc was able to predict occurrence and magnitude of time-series SNA with a higher degree of accuracy ($r^2 = 0.9$, Fig. 10*B*) and reproduce the AP–SNA relationship during closed-loop, drug-induced AP changes (Fig. 10*D*).

Limitations

The present study has several limitations. First, we excluded the efferent effect of the vagally mediated arterial baroreflex, which could affect the properties of baroreflex control of SNAs. Second, artificial respiration and surgical procedures used in this study could affect baroreflex. Third, anaesthetic agents tend to inhibit efferent SNA and depress the gain of baroreflex control of SNA. Fourth, since the present study was animal research, it is limited in its applicability to humans. However, a problem of difficulty in identifying the 'closed-loop' system in contrast with the 'open-loop' system is common in animal and human studies. Lastly, we perfused the carotid sinuses with physiological saline pre-equilibrated with atmospheric. Local hypoxia could have occurred and somewhat affected baroreflex control of SNA. Further research to examine the relevance of the present findings to true physiological conditions is necessary.

Summary

In summary, the open-loop baroreflex transfer functions for the neural and peripheral arcs allowed good prediction of the time-series SNA and AP outputs from baroreceptor pressure and SNA inputs, respectively. In contrast, the closed-loop-spontaneous baroreflex transfer function for the neural arc deviated greatly from the open-loop transfer function, and could not predict the time-series SNA dynamics. However, the closed-loop-spontaneous baroreflex transfer function for the peripheral arc partially matched the open-loop transfer function, with reasonable predictability of the time-series AP dynamics although slightly inferior in accuracy. Furthermore, the predictabilities of open-loop and closed-loop-spontaneous transfer functions of the neural arc were validated by closed-loop pharmacological (phenylephrine and nitroprusside infusions) pressure interventions. Time-series SNA responses to drug-induced AP changes predicted by the open-loop transfer function matched closely the measured responses, whereas SNA responses predicted by the closed-loop-spontaneous transfer function deviated greatly and were the inverse of measured responses. Therefore, although the spontaneous baroreflex transfer function obtained by closed-loop analysis has been believed to represent the neural arc function, it is inappropriate for system identification of the neural arc but is partially appropriate for system identification of the peripheral arc under resting condition, compared with open-loop analysis.

Appendix A

In a block diagram of the open-loop baroreflex system (Fig. 1*A*), CSP is independent of systemic AP because of vascular isolation of the carotid-sinus regions. In this framework, input–output relationships of these arcs are expressed in the frequency domain as:

$$\mathrm{SNA}(f) = H_\mathrm{n}(f) \cdot \mathrm{CSP}(f) + \mathrm{NN}(f) \quad \text{(A1)}$$

$$\mathrm{AP}(f) = H_\mathrm{p}(f) \cdot \mathrm{SNA}(f) + \mathrm{PN}(f) \quad \text{(A2)}$$

where CSP(f), SNA(f) and AP(f) are the fast Fourier transforms of CSP, SNA and systemic AP, respectively. $H_\mathrm{n}(f)$ and $H_\mathrm{p}(f)$ denote the neural arc and the peripheral arc transfer functions, respectively. NN(f) and PN(f) represent unknown noise in the neural and peripheral arcs, respectively.

In the neural arc, calculating the ensemble averages of cross-powers between the terms of eqn (A1) and CSP(f) yields

$$E[\mathrm{SNA}(f) \cdot \mathrm{CSP}(f)^*] = H_\mathrm{n}(f) \cdot E[\mathrm{CSP}(f) \cdot \mathrm{CSP}(f)^*] + E[\mathrm{NN}(f) \cdot \mathrm{CSP}(f)^*] \quad \text{(A3)}$$

where $E[]$ indicates an ensemble average operation. CSP(f)* denotes the complex conjugate of CSP(f). As $H_\mathrm{n}(f)$ is supposed to be time invariant during the observation period, $H_\mathrm{n}(f)$ is outside the ensemble average operation. When CSP is a white-noise signal, E[NN(f)·CSP(f)*] diminishes to zero asymptotically because the white noise is statistically independent of any other noise signal. Thus, we can estimate $H_\mathrm{n}(f)$ by the following equation, which we designate $H_{\text{n-open}}(f)$.

$$H_\mathrm{n}(f) = \frac{E[\mathrm{SNA}(f) \cdot \mathrm{CSP}(f)^*]}{E[\mathrm{CSP}(f) \cdot \mathrm{CSP}(f)^*]} = H_{\text{n-open}}(f) \quad \text{(A4)}$$

Similarly, in the peripheral arc, calculating ensemble averages of cross-powers between terms of eqn (A2) and SNA(f) yields

$$E[\mathrm{AP}(f) \cdot \mathrm{SNA}(f)^*] = H_\mathrm{p}(f) \cdot E[\mathrm{SNA}(f) \cdot \mathrm{SNA}(f)^*] + E[\mathrm{PN}(f) \cdot \mathrm{SNA}(f)^*] \quad \text{(A5)}$$

where SNA(f)* denotes the complex conjugate of SNA(f). As $H_\mathrm{p}(f)$ is supposed to be time invariant during the

observation period, $H_p(f)$ is outside the ensemble average operation. In the open-loop condition, since PN(f) cannot affect SNA(f) and is statistically independent of SNA(f) by definition, E[PN(f)·SNA(f)*] diminishes to zero asymptotically. Thus, we can estimate $H_p(f)$ by the following equation, which we designate $H_{p\text{-open}}(f)$.

$$H_p(f) = \frac{E[\mathrm{AP}(f) \cdot \mathrm{SNA}(f)^*]}{E[\mathrm{SNA}(f) \cdot \mathrm{SNA}(f)^*]} = H_{p\text{-open}}(f) \quad \text{(A6)}$$

In contrast to the open-loop condition, CSP is matched with systemic AP in the closed-loop-spontaneous baroreflex condition (Fig. 1*B*). Thus, the input–output relationships of the arcs in the frequency domain are expressed as:

$$\mathrm{SNA}(f) = H_n(f) \cdot \mathrm{AP}(f) + \mathrm{NN}(f) \quad \text{(A7)}$$

$$\mathrm{AP}(f) = H_p(f) \cdot \mathrm{SNA}(f) + \mathrm{PN}(f) \quad \text{(A8)}$$

In the neural arc, calculating ensemble averages of cross-powers between the terms of eqn (A7) and AP(f) yields

$$E[\mathrm{SNA}(f) \cdot \mathrm{AP}(f)^*] = H_n(f) \cdot E[\mathrm{AP}(f) \cdot \mathrm{AP}(f)^*] + E[\mathrm{NN}(f) \cdot \mathrm{AP}(f)^*] \quad \text{(A9)}$$

$$H_n(f) = \frac{E[\mathrm{SNA}(f) \cdot \mathrm{AP}(f)^*]}{E[\mathrm{AP}(f) \cdot \mathrm{AP}(f)^*]} - \frac{E[\mathrm{NN}(f) \cdot \mathrm{AP}(f)^*]}{E[\mathrm{AP}(f) \cdot \mathrm{AP}(f)^*]} \quad \text{(A10)}$$

However, in the baroreflex closed-loop conditions, the unknown noise in SNA (NN) can affect AP through the peripheral arc transfer function (H_p). In other words, AP(f) inevitably correlates with NN(f), and E[NN(f)·AP(f)*] does not diminish to zero. $H_n(f)$ cannot be determined because the unknown noise NN is practically impossible to quantify. Therefore in protocol 3, we simplify eqn (A10) by neglecting the last term, and define the closed-loop-spontaneous transfer function by the following equation, which we designate $H_{n\text{-closed-spon}}(f)$.

$$H_n(f) = \frac{E[\mathrm{SNA}(f) \cdot \mathrm{AP}(f)^*]}{E[\mathrm{AP}(f) \cdot \mathrm{AP}(f)^*]} = H_{n\text{-closed-spon}}(f) \quad \text{(A11)}$$

However, from eqns (A4) and (A11), it is evident that $H_{n\text{-closed-spon}}(f)$ should be different from $H_{n\text{-open}}(f)$ when NN(f) is large and cannot be neglected.

In the peripheral arc, calculating ensemble averages of cross-powers between the terms of eqn (A8) and SNA(f) yields:

$$E[\mathrm{AP}(f) \cdot \mathrm{SNA}(f)^*] = H_p(f) \cdot E[\mathrm{SNA}(f) \cdot \mathrm{SNA}(f)^*] + E[\mathrm{PN}(f) \cdot \mathrm{SNA}(f)^*] \quad \text{(A12)}$$

$$H_p(f) = \frac{E[\mathrm{AP}(f) \cdot \mathrm{SNA}(f)^*]}{E[\mathrm{SNA}(f) \cdot \mathrm{SNA}(f)^*]} - \frac{E[\mathrm{PN}(f) \cdot \mathrm{SNA}(f)^*]}{E[\mathrm{SNA}(f) \cdot \mathrm{SNA}(f)^*]} \quad \text{(A13)}$$

However, in the baroreflex closed-loop conditions, the unknown noise in AP (PN) can affect SNA through the neural arc transfer function (H_n). In other words, SNA(f) inevitably correlates with PN(f), and E[PN(f)·SNA(f)*] does not diminish to zero. $H_p(f)$ cannot be determined because the unknown noise PN is practically impossible to quantify. Therefore in protocol 3, we simplify eqn (A13) by neglecting the last term and define the closed-loop-spontaneous transfer function by the following equation, which we designate $H_{p\text{-closed-spon}}(f)$.

$$H_p(f) = \frac{E[\mathrm{AP}(f) \cdot \mathrm{SNA}(f)^*]}{E[\mathrm{SNA}(f) \cdot \mathrm{SNA}(f)^*]} = H_{p\text{-closed-spon}}(f) \quad \text{(A14)}$$

However, from eqns (A6) and (A14), it is evident that $H_{p\text{-closed-spon}}(f)$ should be different from $H_{p\text{-open}}(f)$ when PN(f) is large and cannot be neglected.

Appendix B

In rabbits, the transfer function of the baroreflex neural arc (baroreceptor pressure/CSP to SNA) approximates derivative characteristics in the frequency range below 0.8 Hz, and high-cut characteristics of frequencies above 0.8 Hz (Kawada *et al.* 2002). Therefore, according to our previous study, we model the neural arc transfer function (H_n) using eqn (B1) as follows

$$H_n(f) = -K_n \frac{1 + \frac{f}{f_{c1}}j}{\left(1 + \frac{f}{f_{c2}}\right)^2} \exp(-2\pi f j L) \quad \text{(B1)}$$

where f and j represent the frequency (in Hz) and imaginary units, respectively; K_n is static gain (in a.u. mmHg^{-1}); f_{c1} and f_{c2} ($f_{c1} < f_{c2}$) are corner frequencies (in Hz) for derivative and high-cut characteristics, respectively; and L is a pure delay (in s), that would represent the sum of delays in synaptic transmission in the baroreflex central pathways and the sympathetic ganglion. The dynamic gain increases in the frequency range from f_{c1} to f_{c2}, and decreases above f_{c2}. Based on the measured results, we set K_n, f_{c1}, f_{c2} and L at 1, 0.1, 0.8 and 0.2, respectively, in all simulations in Fig. 11.

In addition, the transfer function of the baroreflex peripheral arc (SNA to systemic AP) approximates the second-order low-pass filter with a lag time in rabbits (Kawada *et al.* 2002). Therefore, we model the peripheral

arc transfer function (H_p) using eqn (B2) as follows:

$$H_p(f) = \frac{K_p}{1 + 2\zeta\frac{f}{f_N}j + \left(\frac{f}{f_N}j\right)^2} \exp(-2\pi f j L) \quad \text{(B2)}$$

where K_p is static gain (in mmHg a.u.$^{-1}$); fN and ζ indicate a natural frequency (in Hz) and a damping ratio, respectively; and L is a pure delay (in s) that would represent the sum of delays in synaptic transmission in the neuroeffector junction and intracellular signal transduction in the effector organs. Based on the measured results, we set K_p, f_N, ζ and L at 1, 0.07, 1.4 and 1.0, respectively, in all simulations in Fig. 11.

References

Barres C, Cheng Y & Julien C (2004). Steady-state and dynamic responses of renal sympathetic nerve activity to air-jet stress in sinoaortic denervated rats. *Hypertension* **43**, 629–635.

Brychta RJ, Shiavi R, Robertson D, Biaggioni I & Diedrich A (2007). A simplified two-component model of blood pressure fluctuation. *Am J Physiol Heart Circ Physiol* **292**, H1193–H1203.

Cooke WH, Hoag JB, Crossman AA, Kuusela TA, Tahvanainen KU & Eckberg DL (1999). Human responses to upright tilt: a window on central autonomic integration. *J Physiol* **517**, 617–628.

Cooke WH, Rickards CA, Ryan KL, Kuusela TA & Convertino VA (2009). Muscle sympathetic nerve activity during intense lower body negative pressure to presyncope in humans. *J Physiol* **587**, 4987–4999.

deBoer RW, Karemaker JM & Strackee J (1987). Hemodynamic fluctuations and baroreflex sensitivity in humans: a beat-to-beat model. *Am J Physiol Heart Circ Physiol* **253**, H680–H689.

DiBona GF & Sawin LL (2003). Frequency response of the renal vasculature in congestive heart failure. *Circulation* **107**, 2159–2164.

DiBona GF & Sawin LL (2004). Effect of renal denervation on dynamic autoregulation of renal blood flow. *Am J Physiol Renal Physiol* **286**, F1209–F1218.

Drummond GB (2009). Reporting ethical matters in *The Journal of Physiology*: standards and advice. *J Physiol* **587**, 713–719.

Eckberg DL & Sleight P (1992). *Human Baroreflexes in Health and Disease*. Oxford University Press, New York.

Guyton A & Harris J (1951). Pressoreceptor-autonomic oscillation: a probable cause of vasomotor waves. *Am J Physiol* **165**, 158–166.

Hart EC, Joyner MJ, Wallin BG, Karlsson T, Curry TB & Charkoudian N (2010). Baroreflex control of muscle sympathetic nerve activity: a nonpharmacological measure of baroreflex sensitivity. *Am J Physiol Heart Circ Physiol* **298**, H816–H822.

Ikeda Y, Kawada T, Sugimachi M, Kawaguchi O, Shishido T, Sato T *et al.* (1996). Neural arc of baroreflex optimizes dynamic pressure regulation in achieving both stability and quickness. *Am J Physiol Heart Circ Physiol* **271**, H882–H890.

Ikeda Y, Sugimachi M, Yamasaki T, Kawaguchi O, Shishido T, Kawada T *et al.* (1995). Explorations into development of a neurally regulated cardiac pacemaker. *Am J Physiol Heart Circ Physiol* **269**, H2141–H2146.

Julius SB & Allan GP (ed.) (2000). *Random Data: Analysis and Measurement Procedures*. John Wiley & Sons, Inc., New York.

Kamiya A, Hayano J, Kawada T, Michikami D, Yamamoto K, Ariumi H *et al.* (2005*a*). Low-frequency oscillation of sympathetic nerve activity decreases during development of tilt-induced syncope preceding sympathetic withdrawal and bradycardia. *Am J Physiol Heart Circ Physiol* **289**, H1758–H1769.

Kamiya A, Kawada T, Mizuno M, Shimizu S & Sugimachi M (2010). Parallel resetting of arterial baroreflex control of renal and cardiac sympathetic nerve activities during upright tilt in rabbits. *Am J Physiol Heart Circ Physiol* **298**, H1966–H1975.

Kamiya A, Kawada T, Yamamoto K, Michikami D, Ariumi H, Miyamoto T *et al.* (2005*b*). Dynamic and static baroreflex control of muscle sympathetic nerve activity (SNA) parallels that of renal and cardiac SNA during physiological change in pressure. *Am J Physiol Heart Circ Physiol* **289**, H2641–H2648.

Kamiya A, Kawada T, Yamamoto K, Mizuno M, Shimizu S & Sugimachi M (2008*a*). Upright tilt resets dynamic transfer function of baroreflex neural arc to minify the pressure disturbance in total baroreflex control. *J Physiol Sci* **58**, 189–198.

Kamiya A, Michikami D, Iwase S & Mano T (2008*b*). Decoding rule from vasoconstrictor skin sympathetic nerve activity to nonglabrous skin blood flow in humans at normothermic rest. *Neurosci Lett* **439**, 13–17.

Kawada T, Li M, Kamiya A, Shimizu S, Uemura K, Yamamoto H & Sugimachi M (2010). Open-loop dynamic and static characteristics of the carotid sinus baroreflex in rats with chronic heart failure after myocardial infarction. *J Physiol Sci* **60**, 283–298.

Kawada T, Zheng C, Yanagiya Y, Uemura K, Miyamoto T, Inagaki M *et al.* (2002). High-cut characteristics of the baroreflex neural arc preserve baroreflex gain against pulsatile pressure. *Am J Physiol Heart Circ Physiol* **282**, H1149–H1156.

Malpas SC & Burgess DE (2000). Renal SNA as the primary mediator of slow oscillations in blood pressure during hemorrhage. *Am J Physiol Heart Circ Physiol* **279**, H1299–H1306.

Ogoh S, Fisher JP, Young CN, Raven PB & Fadel PJ (2009). Transfer function characteristics of the neural and peripheral arterial baroreflex arcs at rest and during postexercise muscle ischemia in humans. *Am J Physiol Heart Circ Physiol* **296**, H1416–H1424.

Orea V, Kanbar R, Chapuis B, Barres C & Julien C (2007). Transfer function analysis between arterial pressure and renal sympathetic nerve activity at cardiac pacing frequencies in the rat. *J Appl Physiol* **102**, 1034–1040.

Rowell LB (1993). *Human Cardiovascular Control*. Oxford University Press, New York.

Zhang R, Zuckerman JH, Iwasaki K, Wilson TE, Crandall CG & Levine BD (2002). Autonomic neural control of dynamic cerebral autoregulation in humans. *Circulation* **106**, 1814–1820.

Author contributions

The experiments were performed at the Department of Cardiovascular Dynamics, National Cerebral and Cardiovascular Center Research Institute. A.K. absolutely contributed to: (1) Conception and design, (2) Collection, analysis and interpretation of data and (3) Drafting the article or revising it critically for important intellectual content. Other authors helped him particularly in (3). All authors approved the final version.

Acknowledgments

This study was supported by a research project promoted by Ministry of Health, Labour and Welfare in Japan (no. H21-nano-ippan-005, H22-nanchi-ippan-142), the Grants-in-Aid for Scientific Research promoted by Ministry of Education, Culture, Sports, Science and Technology in Japan (no. 20390462, 22791559) and the Industrial Technology Research Grant Program from New Energy and Industrial Technology Development Organization (NEDO) of Japan.

Heart Vessels (2011) 26:267–273
DOI 10.1007/s00380-010-0054-8

ORIGINAL ARTICLE

Effects of various doses of aspirin on platelet activity and endothelial function

Takashi Furuno · Fumiyasu Yamasaki · Takeshi Yokoyama · Kyoko Sato · Takayuki Sato · Yoshinori Doi · Tetsuro Sugiura

Received: 21 April 2009 / Accepted: 23 April 2010 / Published online: 10 November 2010

Abstract Although aspirin has become an established medicine for cardiac and cerebrovascular diseases, the optimal dose remains unknown. We evaluated the optimal dose of aspirin on platelet activity and endothelial function by administering 11 healthy male volunteers (32 ± 6 years of age) doses of aspirin that were increased in a stepwise manner (0, 81, 162, 330 and 660 mg/day) every 3 days. Platelet activity was assessed as surface P-selectin expression (%) measured by flow cytometry and the platelet aggregation ratio. Endothelial function in the brachial artery was assessed by measuring flow-mediated dilation (FMD) before and after reactive hyperemia. Platelet aggregation and P-selectin expression were significantly and dose-dependently suppressed (81–660 mg), and the FMD ratio tended to increase from 0 to 162 mg, but decreased significantly at 660 mg. In conclusion, although aspirin suppressed platelet activity and even surface P-selectin expression, higher doses worsened endothelial-mediated arterial dilation.

T. Furuno · K. Sato · Y. Doi
Medicine and Geriatrics, Kochi Medical School,
Nankoku, Kochi 783-8505, Japan

F. Yamasaki (✉) · T. Sugiura
Clinical Laboratory, Kochi Medical School,
Nankoku, Kochi 783-8505, Japan
e-mail: yamasakf-kochimed@umin.net

T. Yokoyama
Anesthesiology, Kochi Medical School,
Nankoku, Kochi 783-8505, Japan

T. Sato
Cardiovascular Control, Kochi Medical School,
Nankoku, Kochi 783-8505, Japan

Keywords Aspirin dose · Platelet activity · Endothelial function · Flow-mediated dilation

Introduction

Aspirin is established as a primary and secondary antiplatelet treatment for cardiovascular disease [1–5]. The recommended long-term daily dose of aspirin is 75–150 mg, which is considered to be at least as effective as higher doses [6]. Reports have indicated that higher doses of aspirin are ineffective because of bleeding complications [7–9] and impaired endothelial function [10–12]. Aspirin inhibits the synthesis of thromboxane A2 in platelets and of prostaglandin I2 in endothelial cells. Low dose aspirin only inhibits thromboxane A2 in platelets, whereas a high dose inhibits both. The inhibition of prostaglandin I2 synthesis in endothelial cells would increase the incidence of thromboembolic events [10–12]. However, the effects of optimal doses of aspirin on simultaneous platelet activation and endothelial function in humans remain obscure. One reason for this is that although platelet activation can be evaluated using the platelet aggregation test, a clinical method to evaluate prostaglandin I2 inhibition in endothelial cells remains to be established.

Endothelial function has recently been evaluated as flow-mediated dilation before and after reactive hyperemia [13], and endothelial dysfunction is apparent in patients with cardiovascular and metabolic diseases [14–19]. Although flow-mediated dilation after reactive hyperemia is mainly mediated by NO synthesized in the endothelia [20, 21], another pathway associated with prostacyclin and thromboxane A2 mediates vascular reactivity [22–24]. High dose of aspirin could affect this pathway, leading to vascular relaxation. The present study examines the effects

of various doses of aspirin on platelet activity and endothelial function in healthy humans to determine the optimal dose of aspirin required to suppress platelet aggregation and function.

Subjects and methods

Subjects

We enrolled 11 healthy male volunteers, aged 23–39 years (mean = 32 ± 6 years), with no evidence of heart disease according to a physical examination, standard 12-lead electrocardiography, chest radiography and echocardiography. None of the participants had hypertension, hypercholesteremia, diabetes mellitus or renal disease. All were in sinus rhythm and had not taken any medication for at least 14 days. Each of them provided written, informed consent to participate in the study, the protocol for which was approved by the Local Ethics Committee of Kochi Medical School.

Study protocol

Doses of aspirin (Bufferin 81 or 330 mg/tablet, Lion Co.) were increased (0, 81, 162, 330 and 660 mg) in a stepwise fashion every 3 days for 13 days. Platelet activation and endothelial function were measured at 11:00 a.m. before taking aspirin on the last day of each dose. The participants laid on a bed in a temperature-controlled quiet room, and venous blood was withdrawn from the left forearm vein. Endothelial function was measured in the right arm 30 min after blood collection. The participants did not exercise, consume beverages containing caffeine, high-fat foods or vitamin C, or use tobacco products for at least 4 h before the study.

Endothelial function

Endothelial function was assessed in the brachial artery by measuring flow-mediated dilation before and after reactive hyperemia. Data acquisition and analysis proceeded as described [13]. Briefly, the brachial artery of the right arm was imaged by high-resolution ultrasound (Acuson Sequoia 512) with a 10-MHz linear probe supported by a stereotactic clamp. We selected the B mode longitudinal section of the distal brachial artery, and the M-mode image was magnified using a resolution box function. Vertical internal diameter at end diastole gated by ECG was measured at rest for baseline. A tourniquet placed distally around the ipsilateral forearm was inflated to 250 mmHg for 4.5 min to induce reactive hyperemia. After rapid release, the inner diameter was measured 55 s later. The diameter was measured before and after hyperemia. The FMD ratio (%) was calculated as: 100 × (after diameter − before diameter)/before diameter. Scans were stored and analyzed by two independent observers.

Platelet aggregation test

Platelet function was determined as maximal platelet aggregation rate; that is, platelet-rich-plasma (PRP) was prepared from each participant. To minimize platelet activation during blood collection, blood was withdrawn using a 21-G butterfly needle without a tourniquet. The first 2 ml of blood was discarded, and then 20 ml of blood was transferred into polypropylene tubes containing sodium citrate (3.8%, 1 volume for 9 volumes of blood). We then prepared PRP by centrifugation at $120\times g$ for 10 min at room temperature. Platelet-poor plasma for control to compare PRP aggregation was obtained after re-centrifugation at $1{,}710\times g$ for 15 min.

Platelet aggregation was induced by adenosine diphosphate (ADP) (final concentration of 1.0 or 5.0 μmol/l, MC Medical, Tokyo, Japan) or by collagen (final concentration of 0.25 or 2 μg/ml, MC Medical). The time course of % transmission was measured (MCM HEMA TRACER 212TM; MC Medical), and the maximal platelet aggregation rate was calculated [25, 26].

Measurements of P-selectin (CD62P) and PNC levels

Samples were prepared, and levels of platelet P-selectin (CD62P) and PNC were measured as described [27, 28]. The sample used was the same blood that was collected for the platelet aggregation test. After the first 2 ml of blood was discarded, 2 ml of blood was collected and immediately added to 200 μl of sodium citrate (3.13%). All antibodies were purchased as follows: Fluorescein isothiocyanate (FITC) labeled IgG1 anti-CD62P from Dainippon Pharmaceutical, Osaka; phycoerythin (PE) labeled IgG2a anti-CD42b and FITC labeled IgG1 anti-CD11b from Beckman Coulter, Fullerton. As negative controls, FITC labeled IgG1 (Beckman Coulter, Fullerton) and double-stained (FITC/PE) IgG1 and IgG2a (Dako, High Wycombe) irrelevant antibodies were included. Blood samples were analyzed (EPICS XL Profile Flow Cytometer, Coulter, Miami, FL) using either one or two fluorochromes.

To prepare samples for measurements of platelet CD62P levels, blood (5 μl) was added to round-bottomed polystyrene tubes containing 50 μl platelet buffer (10 mmol/l HEPES, 145 mmol/l NaCl, 5 mmol/l KCl, 1 mmol/l $MgSO_4$, pH 7.4), and 5 μl of anti-CD62P or control IgG1 antibody. The samples were gently suspended and incubated in the dark at room temperature for 20 min without stirring. Then 250-μl fixative (Beckman Coulter, Fullerton,

9.25% formaldehyde) was added, and the tubes were incubated for a further 10 min. The samples were then diluted with 500 μl of buffer and analyzed by flow cytometry within 1 h of fixation. In flow cytometric analysis, the peaks emission intensity of FITC and phycoerythrin fluorescence were detected at 515 and 580 nm, respectively. After forward and side scatter was measured with the gain setting in logarithmic mode, platelet sized events were counted. CD62P positive platelets were defined as those with a fluorescence intensity exceeding that of 98% of the platelets stained with control antibody.

To prepare samples for the PNC measurements, blood (50 μl) was added to round-bottomed polystyrene tubes containing 5 μl each of anti-CD42b and anti-CD11b (platelet and neutrophil markers, respectively) or isotype control antibodies. The samples were gently mixed and incubated in the dark at room temperature for 10 min without stirring. Then 500 μl of fixative was added, and the tubes were incubated for a further 10 min. Flow cytometry proceeded within 1 h of preparation. After forward and side scatter were measured with the gain setting in linear mode, neutrophil-sized events were selected. Results were defined as positive when the fluorescence intensity exceeded that of the isotype matched (IgG1 and IgG2a) control antibody staining (98%). Both CD11b and CD42b positive events that were considered PNCs were expressed as ratios (%) of events with positive CD11b staining of those of whole neutrophils. We evaluated the ability of the platelets to be activated, i.e., platelet activation reserve in the presence of 5 μl of ADP (5 μmol/l).

We also counted blood cells and measured coagulation factors of prothrombin time (PT), activated partial thromboplastin time (APTT) and fibrinogen.

Statistical analysis

Data are presented as means ± SEM. Group means for each parameter were determined and compared using the analysis of variance (ANOVA) repeated measures, with the post-hoc Tukey–Kramer test. A value of $p < 0.05$ was considered to represent statistical significance.

Results

Aspirin administration did not alter the white blood cells, red blood cells, hemoglobin, hematocrit or platelet counts in the blood. The coagulation factors, PT and APTT, did not change significantly before and after aspirin administration. However, maximal platelet aggregation rates in the presence of ADP (5.0 μmol/l) or collagen (2 μg/ml) were significantly reduced from the baseline level after all doses of aspirin (81, 162, 330 and 660 mg): ADP; 78 ± 3–67 ± 2, 66 ± 2, 65 ± 2, 66 ± 2%, all ps < 0.01; collagen; 85 ± 2–34 ± 6, 38 ± 6, 34 ± 5, 35 ± 6%, all ps < 0.01. The effects on P-selectin, P-selectin with ADP and PNC with ADP tended to be similar (Table 1; Fig. 1), whereas PNC showed no tendency. Therefore, aspirin of any dose over 81 mg/day suppressed platelet activity.

Blood pressure was 121 ± 8/68 ± 8 at baseline and 127 ± 9/71 ± 8 at the end of the study, showing no significant change. At any dose of aspirin, heart rate at each measurement of FMD did not change significantly. Although arterial diameter did not significantly change after hyperemia, the FMD ratio (%) tended to increase at a dose of 81 mg (1.68 ± 0.29–2.78 ± 0.47, $p = 0.08$) and significantly increased at 162 mg (3.67 ± 0.41, $p < 0.05$) compared with the baseline without aspirin. The FMD ratio then tended to decrease at a dose of 330 mg (3.30 ± 0.50, n.s.) from 162 mg, but tended to be higher compared with the baseline ($p = 0.07$). The FMD ratio further decreased at a dose of 660 mg (1.07 ± 0.34) compared with that at either 162 or 330 mg ($p < 0.01$, $p < 0.01$, respectively), and tended to be lower from baseline or at a dose of 81 mg (Table 1; Fig. 1). Therefore, the optimal dose of aspirin for endothelial function assessed by the FMD ratio was 162 mg per day.

Discussion

The major finding of this study was that aspirin at any daily dose over 81 mg suppressed platelet activity and that the optimal dose of endothelial function was 162 mg/day. However, 660 mg/day of aspirin worsened endothelial function.

Aspirin plays an important role in the primary and secondary prevention of cardiovascular events, and it has remained the most cost-effective clinical drug for over 3 decades [1–6]. Reports indicate that a daily dose of 75–150 mg is just as effective as higher doses. An initial loading dose of at least 150 mg aspirin might be required in acute settings, but the effects of daily doses of <75 mg have been less certain, and doses of >1,000 mg daily are not recommended due to bleeding side effects [7–9].

The recent findings of the Antithrombotic Trialists' Collaboration meta-analysis of patients with previous thrombotic events or other predisposing conditions showed that aspirin reduces the total risk for cardio-cerebral vascular events by 22% [6]. From the viewpoint of the daily aspirin dose, the proportional reduction in vascular events was 19% at 500–1,500 mg/day, 26% at 160–325 mg/day and 32% at 75–150 mg/day. Although the effects of aspirin doses of ≥ or <75 mg in a direct comparison did not significantly differ, doses of <75 mg/day seemed to have somewhat reduced

Table 1 Blood cell count, coagulation factor, platelet activity and endothelial function

Aspirin dose (mg/day)	0	81	162	330	660
Blood cell count					
RBC ($\times 10^4/\mu l$)	490 ± 7	483 ± 10	483 ± 8	483 ± 8	486 ± 7
Hemoglobin (g/dl)	15.2 ± 0.1	15.2 ± 0.2	14.9 ± 0.2	15.0 ± 0.2	14.7 ± 0.2
Hematocrit (%)	44.5 ± 0.3	44.6 ± 0.5	43.8 ± 0.6	44.3 ± 0.6	43.1 ± 0.6
Platelet ($\times 10^4/\mu l$)	26.5 ± 1.4	25.1 ± 1.0	24.3 ± 0.9	24.6 ± 1.1	24.7 ± 0.9
WBC (μl^{-1})	5.70 ± 0.42	5.84 ± 0.34	5.84 ± 0.34	5.74 ± 0.34	6.29 ± 0.56
Coagulation factor					
PT (s)	10.4 ± 0.1	10.3 ± 0.1	10.3 ± 0.1	10.2 ± 0.1	10.1 ± 0.1
PT (%)	95.7 ± 4.0	98.3 ± 5.1	96.3 ± 3.3	99.7 ± 3.1	105.2 ± 5.4
INR	1.03 ± 0.03	1.02 ± 0.03	1.03 ± 0.02	1.01 ± 0.02	0.98 ± 0.03
APTT (s)	28.1 ± 0.8	27.8 ± 0.5	27.8 ± 0.6	27.7 ± 0.7	27.2 ± 0.6
APTT (%)	108.5 ± 5.3	109.6 ± 3.8	109.9 ± 4.6	113.0 ± 4.8	116.1 ± 4.3
Fibrinogen (mg/dl)	198.9 ± 14.8	203.8 ± 9.3	200.4 ± 10.2	193.6 ± 8.8	188.1 ± 12.1
Platelet surface marker					
PNC (%)	7.0 ± 0.8	6.4 ± 0.7	6.9 ± 0.7	6.6 ± 0.6	6.0 ± 0.8
PNC (ADP) (%)	17.8 ± 3.1	14.1 ± 2.0	15.5 ± 1.1	14.4 ± 2.5	15.9 ± 3.4
P-selectin (%)	12.9 ± 1.3	10.2 ± 0.4	11.3 ± 0.7	10.4 ± 0.7	10.5 ± 0.5
P-selectin (ADP) (%)	29.6 ± 2.7	26.6 ± 2.2	27.4 ± 2.4	26.2 ± 2.2	27.3 ± 2.2
Platelet maximal aggregation rate					
ADP (5 μmol/l) (%)	78 ± 3	67 ± 2**	66 ± 2**	65 ± 2**	66 ± 2**
ADP (1 μmol/l) (%)	31 ± 3	32 ± 4	33 ± 4	31 ± 4	33 ± 3
Collagen (2 μg/ml) (%)	85 ± 2	34 ± 6**	38 ± 6**	34 ± 5**	35 ± 6**
Collagen (0.25 μg/ml) (%)	23 ± 8	7 ± 2	8 ± 2	8 ± 1	7 ± 1
Endothelial function					
Diameter (before) (%)	0.367 ± 0.013	0.386 ± 0.014	0.375 ± 0.012	0.379 ± 0.013	0.379 ± 0.010
Heart rate (before) (bpm)	77 ± 10	76 ± 7	75 ± 8	72 ± 8	73 ± 7
Diameter (after) (%)	0.374 ± 0.013	0.396 ± 0.013	0.388 ± 0.013	0.391 ± 0.013	0.382 ± 0.009
Heart rate (after) (bpm)	77 ± 10	78 ± 9	73 ± 12	71 ± 8	73 ± 6
FMD ratio (%)	1.68 ± 0.29	2.78 ± 0.47	3.67 ± 0.41*	3.30 ± 0.50	1.07 ± 0.34$^{\#\$}$

Values are mean ± SE

RBC red blood cells, *WBC* white blood cells, *ADP* adenosine diphosphate, *PT* prothrombin time, *INR* international normalized ratio, *APTT* activated partial thromboplastin time, *PNC* platelet neutrophil complexes, *FMD* flow-mediated dilation

* $p < 0.05$ and ** $p < 0.01$ compared with baseline value (0 mg); $^{\#}$ $p < 0.01$ and $^{\$}$ $p < 0.01$ compared with values at 162 and 330 mg aspirin, respectively

effects (proportional reduction 13%). However, trials that examined doses of aspirin of ≥75 mg/day found a significant reduction in cardiovascular events, whereas three trials using doses of <75 mg/day did not. Similarly, a recent large trial of aspirin in primary prevention among women did not demonstrate a benefit of very-low-dose aspirin (100 mg every other day) [29]. No evidence supports the notion that daily aspirin doses of >1,000 mg is preferable for the prevention of serious vascular events among patients at high risk of stroke [7, 8]. One study found that the risk of the composite outcome of myocardial infarction, stroke or death within 3 months of carotid endarterectomy was significantly lower among patients taking 81 or 325 than 625–1,300 mg of aspirin daily [9]. In the present study, aspirin at doses above 81 mg suppressed platelet activity assessed by the aggregation test, P-selectin and PNC levels. This result is consistent with previous reports that show aspirin at even the low dose of 81 mg exerts antiplatelet effects.

Higher doses of aspirin can cause bleeding complication [7–9] and also impair endothelial function, which is known as the "aspirin dilemma" [10–12]. Aspirin inhibits a production of thromboxane A2 and cyclo-oxygenase enzyme, which synthesize thromboxane A2, a potent platelet aggregator in the platelets. Therefore, inhibiting thromboxane A2 is anti-thrombotic. Aspirin also inhibits cyclo-oxygenase enzyme in vascular endothelial cells, which is the source of prostaglandin I2, a vasodilator. A high dose of aspirin achieves both platelet inhibition

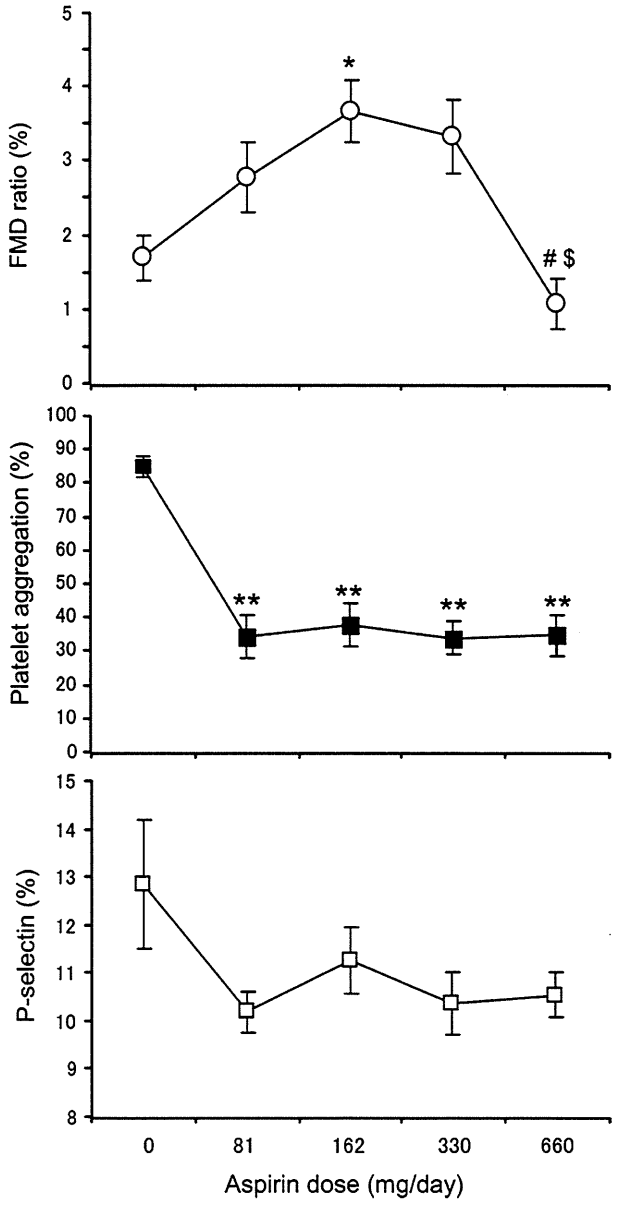

Fig. 1 FMD ratios (*upper panel*), maximal platelet aggregation rates (*middle panel*) and P-selectin levels (*lower panel*). Values are means ± SE. *FMD* Flow-mediated dilation. $^{*}p < 0.05$ from baseline (0 mg), $^{\#}p < 0.01$ from value at aspirin 162 mg, $^{\$}p < 0.01$ from value at 330 mg

and vasodilation, whereas a low dose spares endothelial cyclo-oxygenase activity and vasodilation. Therefore, the inhibition of prostaglandin I2 synthesis in the endothelial cells would increase the incidence of thromboembolic events. However, no clinical studies have examined endothelial function at various doses of aspirin, because endothelial function cannot be evaluated to determined platelet activity in a clinical setting. Endothelial function has recently been evaluated noninvasively as FMD to stratify patients according to cardiovascular risk, and endothelial dysfunction is associated with a poor prognosis [14–19]. Although a direct mechanism of decreased a FMD ratio at high dose of aspirin is uncertain, this could be due to high dose aspirin affecting vasodilation via endothelial cyclo-oxygenase inhibition.

Although FMD after reactive hyperemia is mainly mediated by NO synthesized in the endothelia [20, 21], another pathway associated with prostacyclin and thromboxane A2 mediates vascular reactivity [22–24]. Husain et al. [22] showed aspirin modulates acetylcholine-induced peripheral vasodilatation in patients with coronary atherosclerosis, and this effect may be due to the inhibition of vasoconstriction induced by one or more cyclo-oxygenases. Sun et al. [23] also showed that FMD is mediated by endothelium-derived prostanoids as it is blocked by indomethacin in eNOS knockout mice. Furthermore, Taubert et al. [24] showed a therapeutically relevant concentration of aspirin elicits NO release from the vascular endothelium independently of cyclo-oxygenase inhibition in in vitro study. These findings showed low dose aspirin could improve endothelial dysfunction and increase FMD. On the other hand, Gori et al. [30] reported 500 mg aspirin (once oral) did not affect the FMD ratio, but it significantly blunted low-flow-mediated constriction of the resting arterial tone. The difference from our results may be due to the dose and period of aspirin intake.

We found here that the FMD ratio increased at 162 mg from the baseline level without aspirin, and that this significantly decreased at a dose of 660 mg from that of 162 or 330 mg. Thus, low dose aspirin (<330 mg) did not deteriorate endothelial function, and 81 mg was sufficient to suppress platelet activity in healthy volunteers. However, platelets are more activated in patients with atherosclerosis than in normal individuals [31], and patients with atherosclerosis have endothelial dysfunction [14–19]. Moreover, several studies have indicated that patients at risk for atherosclerosis were less sensitive to the platelet inhibitory effect of aspirin [32–36]. Therefore, the optimal dose of aspirin might differ among patients with atherosclerosis compared with normal individuals, and aspirin doses of >81 mg might be required.

Platelet aggregation tests and FMD measurement might comprise an easy and noninvasive tool to determine the optimal dose of aspirin for such patients in a clinical setting. We applied the platelet aggregation test with light transmittance aggregometry and direct P-selectin measurements. Levels of platelet inhibition might be determined by evaluating several critical pathways [37]. That study used a new device based on light transmittance aggregometry that measures platelet activity more rapidly than classical devices and that could guide the choice of antiplatelet therapies. This method can evaluate patients

with aspirin resistance and optimize the dose, but cannot evaluate the extent to which various aspirin doses affect the endothelial function. On the other hand, FMD can evaluate the endothelial function affected by aspirin and generate useful information that could improve clinical outcomes.

Finally, the sample size in this study was small, and the subjects were normal male volunteers. Patients with atherosclerotic disease might have more activated platelets than normal individuals. Further studies are needed with a larger number of normal individuals and a cohort of patients with atherosclerotic disease.

Acknowledgments We thank Tadashi Ueta for excellent technical assistance. We also thank Misa Nakagawa, Yanan Zhang and Dongmei Zhang for technical assistance throughout the study.

References

1. Elwood PC, Cochrane AL, Burr ML, Sweetnam PM, Williams G, Welsby E, Hughes SJ, Renton R (1974) A randomized controlled trial of acetyl salicylic acid in the secondary prevention of mortality from myocardial infarction. Br Med J 1:436–440
2. Steering Committee of the Physicians' Health Study Research Group (1989) Final report on the aspirin component of the ongoing Physicians' Health Study. N Engl J Med 321:129–135
3. Peto R, Gray R, Collins R, Wheatley K, Hennekens C, Jamrozik K, Warlow C, Hafner B, Thompson E, Norton S, Gilliland J, Doll R (1988) Randomised trial of prophylactic daily aspirin in British male doctors. Br Med J (Clin Res Ed) 296(6618):313–316
4. Hebert PR, Hennekens CH (2000) An overview of the four randomized trials of aspirin therapy in the primary prevention of vascular disease. Arch Intern Med 160:3123–3127
5. Kubota N, Kasai T, Miyauchi K, Njaman W, Kajimoto K, Akimoto Y, Kojima T, Ken Y, Takeshi K, Hiroyuki D (2008) Therapy with statins and aspirin enhances long-term outcome of percutaneous coronary intervention. Heart Vessels 23:35–39
6. Antithrombotic Trialists' Collaboration (2002) Collaborative meta-analysis of randomised trials of antiplatelet therapy for prevention of death, myocardial infarction, and stroke in high risk patients. Br Med J 324:71–86
7. Dyken ML, Barnett HJ, Easton JD, Fields WS, Fuster V, Hachinski V, Norris JW, Sherman DG (1992) Low-dose aspirin and stroke. "It ain't necessarily so". Stroke 23:1395–1399
8. Barnett HJ, Kaste M, Meldrum H, Eliasziw M (1996) Aspirin dose in stroke prevention: beautiful hypotheses slain by ugly facts. Stroke 27:588–592
9. Taylor DW, Barnett HJ, Haynes RB, Ferguson GG, Sackett DL, Thorpe KE, Simard D, Silver FL, Hachinski V, Clagett GP, Barnes R, Spence JD (1999) Low-dose and high-dose acetylsalicylic acid for patients undergoing carotid endarterectomy: a randomised controlled trial. ASA and Carotid Endarterectomy (ACE) Trial Collaborators. Lancet 353:2179–2184
10. Moncada S, Gryglewski R, Bunting S, Vane JR (1976) An enzyme isolated from arteries transforms prostaglandin endoperoxides to an unstable substance that inhibits platelet aggregation. Nature 263:663–665
11. Willems C, De Groot PG, Pool GA, Gonsalvez MS, Van Aken WG, Van Mourik JA (1982) Arachidonate metabolism in cultured human vascular endothelial cells. Evidence for two prostaglandin synthetic pathways sensitive to acetylsalicylic acid. Biochim Biophys Acta 713:581–588
12. Ozturk O, Greaves M, Templeton A (2002) Aspirin dilemma. Remodelling the hypothesis from a fertility perspective. Hum Reprod 17:1146–1148
13. Corretti MC, Anderson TJ, Benjamin EJ, Celermajer D, Charbonneau F, Creager MA, Deanfield J, Drexler H, Gerhard-Herman M, Herrington D, Vallance P, Vita J, Vogel R, International Brachial Artery Reactivity Task Force (2002) Guidelines for the ultrasound assessment of endothelial-dependent flow-mediated vasodilation of the brachial artery: a report of the International Brachial Artery Reactivity Task Force. J Am Coll Cardiol 39:257–265
14. Witte DR, Westerink J, de Koning EJ, van der Graaf Y, Grobbee DE, Bots ML (2005) Is the association between flow-mediated dilation and cardiovascular risk limited to low-risk populations? J Am Coll Cardiol 45:1987–1993
15. Dogra G, Rich L, Stanton K, Watts GF (2001) Endothelium-dependent and independent vasodilation studies at normoglycaemia in type I diabetes mellitus with and without microalbuminuria. Diabetologia 44:593–601
16. Yeboah J, Crouse JR, Hsu FC, Burke GL, Herrington DM (2007) Brachial flow-mediated dilation predicts incident cardiovascular events in older adults: the Cardiovascular Health Study. Circulation 115:2390–2397
17. Mizia-Stec K, Gasior Z, Zahorska-Markiewicz B, Holecki M, Haberka M, Mizia M, Gomułka S, Zak-Gołab A, Gościńska A (2008) The indexes of arterial structure and function in women with simple obesity: a preliminary study. Heart Vessels 23:224–229
18. Fujii N, Tsuchihashi K, Sasao H, Eguchi M, Miurakami H, Hase M, Higashiura K, Yuda S, Hashimoto A, Miura T, Ura N, Shimamoto K (2008) Insulin resistance functionally limits endothelium-dependent coronary vasodilation in nondiabetic patients. Heart Vessels 23:9–15
19. Crisby M, Kublickiene K, Henareh L, Agewall S (2009) Circulating levels of autoantibodies to oxidized low-density lipoprotein and C-reactive protein levels correlate with endothelial function in resistance arteries in men with coronary heart disease. Heart Vessels 24:90–95
20. Pohl U, Holtz J, Busse R, Bassenge E (1986) Crucial role of endothelium in the vasodilator response to increased flow in vivo. Hypertension 8:37–44
21. Joannides R, Haefeli WE, Linder L, Richard V, Bakkali EH, Thuillez C, Lüscher TF (1995) Nitric oxide is responsible for flow-dependent dilatation of human peripheral conduit arteries in vivo. Circulation 91:1314–1319
22. Husain S, Andrews NP, Mulcahy D, Panza JA, Quyyumi AA (1998) Aspirin improves endothelial dysfunction in atherosclerosis. Circulation 97:716–720
23. Sun D, Huang A, Smith CJ, Stackpole CJ, Connetta JA, Shesely EG, Koller A, Kaley G (1999) Enhanced release of prostaglandins contributes to flow-induced arteriolar dilation in eNOS knockout mice. Circ Res 85:288–293
24. Taubert D, Berkels R, Grosser N, Schröder H, Gründemann D, Schömig E (2004) Aspirin induces nitric oxide release from vascular endothelium: a novel mechanism of action. Br J Pharmacol 143:159–165
25. Born GV (1962) Aggregation of blood platelets by adenosine diphosphate and its reversal. Nature 194:927–929
26. O'brien JR (1962) Platelet aggregation: Part I some effects of the adenosine phosphates, thrombin, and cocaine upon platelet adhesiveness. J Clin Pathol 15:446–452
27. Peters MJ, Heyderman RS, Hatch DJ, Klein NJ (1997) Investigation of platelet-neutrophil interactions in whole blood by flow cytometry. J Immunol Methods 209:125–135
28. Yamasaki F, Furuno T, Sato K, Zhang D, Nishinaga M, Sato T, Doi Y, Sugiura T (2005) Association between arterial stiffness and platelet activation. J Hum Hypertens 19:527–533

29. Ridker PM, Cook NR, Lee IM, Gordon D, Gaziano JM, Manson JE, Hennekens CH, Buring JE (2005) A randomized trial of low-dose aspirin in the primary prevention of cardiovascular disease in women. N Engl J Med 352:1293–1304
30. Gori T, Dragoni S, Lisi M, Di Stolfo G, Sonnati S, Fineschi M, Parker JD (2008) Conduit artery constriction mediated by low flow a novel noninvasive method for the assessment of vascular function. J Am Coll Cardiol 51:1953–1958
31. Cahill MR, Newland AC (1993) Platelet activation in coronary artery disease. Br J Biomed Sci 50:221–234
32. Hung J, Lam JY, Lacoste L, Letchacovski G (1995) Cigarette smoking acutely increases platelet thrombus formation in patients with coronary artery disease taking aspirin. Circulation 92:2432–2436
33. Steinhubl SR, Moliterno DJ (1997) Glycoprotein IIb/IIIa receptor antagonists for the treatment of unstable angina. Heart Vessels Suppl 12:148–155
34. Sacco M, Pellegrini F, Roncaglioni MC, Avanzini F, Tognoni G, Nicolucci A, PPP Collaborative Group (2003) Primary prevention of cardiovascular events with low-dose aspirin and vitamin E in type 2 diabetic patients: results of the Primary Prevention Project (PPP) trial. Diabetes Care 26:3264–3272
35. Blann AD, Dobrotova M, Kubisz P, McCollum CN (1995) von Willebrand factor, soluble P-selectin, tissue plasminogen activator and plasminogen activator inhibitor in atherosclerosis. Thromb Haemost 74:626–630
36. Davì G, Romano M, Mezzetti A, Procopio A, Iacobelli S, Antidormi T, Bucciarelli T, Alessandrini P, Cuccurullo F, Bittolo Bon G (1998) Increased levels of soluble P-selectin in hypercholesterolemic patients. Circulation 97:953–957
37. Cannon CP, McLean DS (2006) Critical pathways using platelet testing to potentially optimize the use of oral antiplatelet therapy. Am J Cardiol 98:33N–38N

Ann Surg Oncol (2011) 18:2042–2047
DOI 10.1245/s10434-010-1499-9

Annals of
SURGICAL ONCOLOGY
OFFICIAL JOURNAL OF THE SOCIETY OF SURGICAL ONCOLOGY

ORIGINAL ARTICLE – TRANSLATIONAL RESEARCH AND BIOMARKERS

Feasibility of ICG Fluorescence-Guided Sentinel Node Biopsy in animal Models using the HyperEye Medical System

Kohichi Yamauchi, MD, PhD[1], Hiroshi Nagafuji, MD[1], Takehiro Nakamura, MD[1], Takayuki Sato, MD, PhD[2], and Naoyuki Kohno, MD, PhD[1]

[1]Department of Otolaryngology, Head and Neck Surgery, Kyorin University School of Medicine, Mitaka, Tokyo, Japan; [2]Department of Cardiovascular Control, Kochi Medical School, Nankoku, Kochi, Japan

ABSTRACT

Background. The sentinel lymph node (SLN) concept is accepted for several types of cancers. Current methods for sentinel node detection involve radioisotopes and blue dye. They have shown good results, but some drawbacks remain. Indocyanine green (ICG) fluorescence using the HyperEye Medical System (HEMS) was evaluated as a new method.

Methods. This was a prospective, nonrandomized, experimental study in four Japanese white rabbits and six Yorkshire pigs. ICG and indigo carmine were injected into the tongue, larynx, or hypopharynx, and ICG fluorescence detection was evaluated using both transcutaneous visualization of lymphatic vessels and intraoperative identification of SLNs.

Results. The SLNs appeared as shining fluorescent spots with HEMS transcutaneously in rabbits, but no SLNs were detected transcutaneously in pigs. Eleven procedures identified SLNs, but one did not due to a technical problem.

Conclusions. HEMS could become useful for predicting lymph node metastasis during surgery for head and neck cancer.

Neck lymph node status is the most important prognostic factor in head and neck cancer, and in recent years, with extensive pathological workups, the sentinel lymph node (SLN) tumor burden has been advocated as a staging measure.[1–3] SLN biopsy is an excellent approach to improve staging of lymph node metastasis.[4–7] Many authors report that both blue dye and/or radioisotope methods are effective for detecting SLNs, but some drawbacks remain.[8–11] The HyperEye Medical System (HEMS) is a new detection device that uses indocyanine green (ICG) fluorescence.[12–15] This device allows both transcutaneous visualization of lymphatic vessels and intraoperative identification of SLNs with simultaneous color and near-infrared images during surgery.

The system was originally developed for cardiovascular surgery by Sato et al.[12] Intraoperative conventional angiography is an invasive procedure for graft assessment, which was developed as a safe way to evaluate graft patency with visual images.

To the best of our knowledge, this is the first study to attempt sentinel node biopsy guided by ICG fluorescence imaging in the head and neck region. We demonstrate the characteristics of this device and compare it to the use of blue dye in animal models.[16–18]

MATERIALS AND METHODS

Design

The objective of this study was to evaluate the feasibility of sentinel node biopsy by a combined fluorescence and dye method for the head and neck region. Six Yorkshire pigs (50 kg) and four Japanese white rabbits (4 kg) were used in this Institutional Animal Care and Use Committee (IACUC) of Kyorin University-approved study.

Description of the HyperEye Medical System

The HEMS (Mizuho Medical Co. Ltd., Tokyo, Japan; Fig. 1) can visualize ICG-enhanced structures with vivid color. It consists of a combination of custom-made optical filters and an ultra-high-sensitivity CCD image sensor with

First Received: 23 June 2010;
Published Online: 5 February 2011

N. Kohno, MD, PhD
e-mail: sukohno@ks.kyorin-u.ac.jp

FIG. 1 HyperEye Medical System

non-Bayer color filter arrays, which can detect visible and near infrared (NIR) rays from 380–1200 nm without a bias in color balance at 30 frames per second.[2,12]

ICG (Daiichi Sankyo Co., Ltd., Tokyo, Japan) is a water-soluble, tricarbocyanine dye with a peak spectral absorption at 760–800 nm when dissolved in blood. Using this technique, the ICG is illuminated with an array of light-emitting diodes (LEDs) at 760 nm, after which it emits light at 830 nm. The HEMS then captures the ICG fluorescence images by a color CCD camera.

Experimental Procedures

Animal Preparation Rabbits were administered 10 mg/kg of Nembutal intravenously. Pigs were premedicated with 0.2 mg/kg of butorphanol, 0.08 mg/kg of medetomidine, and 20 mg/kg of ketamine administered intramuscularly. Endotracheal anesthesia was induced and maintained with 0.5–2% isoflurane. Heart rate, oxygen saturation, and body temperature were monitored.

Administration of ICG and Indigo Carmine ICG (1 ml: 5 mg) and indigo carmine (3 ml; Daiichi Sankyo Co., Ltd., Tokyo, Japan) were mixed to a final solution of 4 ml.[19] The pigs and rabbits were placed in the supine position on the operating table.

FIG. 2 Administration of ICG and indigo carmine. Tracer was injected into the tongue of a pig

Tongue Four rabbits were used. Dye was injected into the 0.5-cm-deep submucosal layer at one site with a 27-G needle. The total amount of injected dye was 1 ml.

Two pigs were used. Tracer was injected into the 0.5-cm-deep submucosal layer at four defined sites with a 23-G needle. The total amount of injected tracer was 2 ml. All pigs were injected into both sides of the tongue (Fig. 2).

Larynx Two pigs were used. Tracers (1 ml each) were injected subcutaneously at a supraglottic site (0.5 cm away from the anterior commissure) and the left vocal cord by laryngeal microsurgery. Laryngeal injections were performed using a laryngoscope (Jackson type, Nagashima Medical Instruments Co., Ltd., Tokyo, Japan) and a grasping forceps (Center sliding type, Nagashima Medical Instruments Co., Ltd.) to guide a 23-G needle to the injection sites. The needle was attached to a 50-cm connection tube and a 5-ml disposable syringe. The laryngoscope was positioned to provide an endoscopic surgical approach, and tracer (1 ml) was injected into 0.2-cm-deep subcutaneous tissue.

Hypopharynx Two pigs were used. Tracer (1 ml) was injected into 0.2-cm-deep subcutaneous tissue at one site of the piriform sinus by laryngeal microsurgery.

SLN Detection with HEMS The HyperEye CCD camera was positioned 50 cm above the area. Subsequently, 10–15 min after the injection, the detection of SLNs as transcutaneous shining fluorescent spots on the TV monitor in a dim room was attempted before beginning the surgical procedure. If the shining fluorescent spots were observed, the surgical procedure was begun under normal room light. A semicircular neck incision was made from both angles of the mandible to the sternal notch and was elevated as a skin flap. Both blue dye and HEMS were used to search for SLNs. SLNs that received indigo carmine were stained

green when examined by the naked eye, whereas SLNs that received ICG appeared as shining fluorescent spots. Shining spots could be landmarks for surgery and facilitate the identification of SLNs. Even if the shining fluorescent spots could not be observed before the beginning of the surgical procedure, SLNs could be identified during surgery, because thick skin was elevated and soft tissues were removed gradually, thus making identification easier. The SLNs were dissected, and then bilateral neck dissections (removal of equivalent to levels I–V) were performed.

RESULTS

Identification of SLNs

The results are shown in Table 1 and described below.

Rabbits

Tongue Four unilateral injections into the ventrolateral tongue were performed in four rabbits. In all procedures, SLNs were detected transcutaneously by HEMS in the unilateral submandibular area (Fig. 3), and they were identified as stained green during surgery. One other SLN was found by HEMS in the lower neck region, but it was not stained with blue dye.

The mean ± standard deviation (SD) number of SLNs identified by HEMS was 1.25 ± 0.5—80% of which was stained with blue dye. No residual blue or contrast-positive nodes were identified on neck dissection.

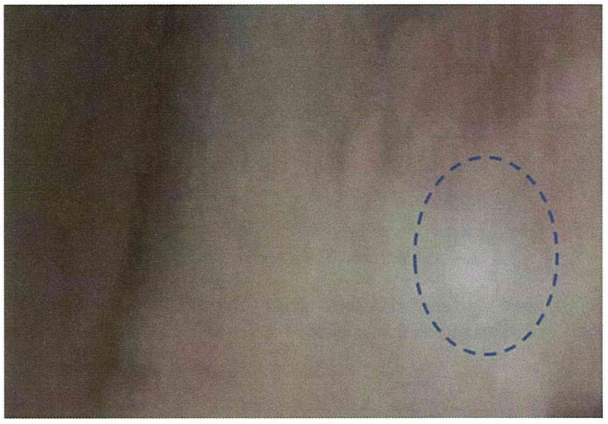

FIG. 3 ICG fluorescence imaging. The SLN of a rabbit is displayed transcutaneously as a shining spot in the *dotted circle*

Pigs

Tongue Two bilateral injections were performed per pig. In all procedures, no SLNs were detected transcutaneously by HEMS. However, during surgery, ten SLNs were identified as shining spots in the submandibular area of the same injection side, 70% of which also was stained green. Figure 4 shows one of ten SLNs (procedure 7 in pig 2).

Larynx

One pig had a supraglottic injection and another had a vocal cord injection. No supraglottic SLNs were detected. The reason for this was that administration of ICG and indigo carmine must have failed; a needle must have

TABLE 1 HEMS and blue dye sentinel node biopsy results

Animal	Procedure	Side	Site	HEMS		Dye	
				Transcutaneous No. of SNL	Intraoperative No. of SNL	No. of SNL	Visibility of lymph vessels
Rabbit 1	1	L	Tongue		1	1	+
Rabbit 2	2	L	Tongue	1	1	1	+
Rabbit 3	3	R	Tongue	1	2	1	+
Rabbit 4	4	R	Tongue	1	1	1	+
Mean ± SD				1 ± 0	1.25 ± 0.5	1 ± 0	
Pig 1	5	L	Tongue	0	4	3	+
	6	R		0	4	2	+
Pig 2	7	L	Tongue	0	1	1	+
	8	R		0	1	1	+
Pig 3	9	C	Larynx (S)	0	0	0	−
Pig 4	10	L	Larynx (v)	0	2	1	+
Pig 5	11	L	Hypopharynx	0	1	1	+
Pig 6	12	R	Hypopharynx	0	1	1	+
Mean ± SD				0 ± 0	1.75 ± 1.33	1.25 ± 0.75	

HEMS HyperEye Medical System, *SNL* sentinel lymph node, *R* right, *L* left, *C* center, *S* supraglottis, *V* vocal cord, *SD* standard deviation

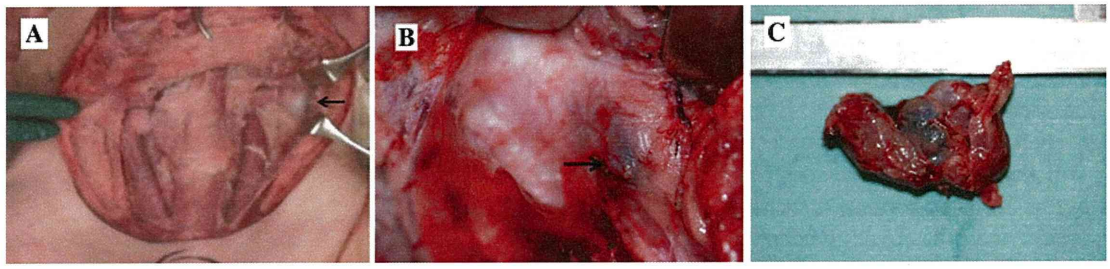

FIG. 4 An SLN (*arrow*) is intraoperatively identified as a shining spot in the submandibular area in the porcine neck by HEMS (**a**), and the naked eye view shows that is stained green (**b**). Excision of the same SLN visibly stained by blue dye (**c**)

penetrated the thyroid cartridge (deeper than 0.2 cm), from which dye subsequently leaked.

In the procedure for the left vocal cord, two SLNs were identified by HEMS in the left paratracheal region during surgery. One of these SLNs was stained by dye.

Hypopharynx

Two unilateral injections into the piriform sinus were performed in two pigs. Two procedures identified a single SLN during surgery in the paratracheal region. Lymphatic flows and SLNs were identified by HEMS in the paratracheal area on the same injection side (Fig. 5).

The mean ± SD number of SLNs was 1.75 ± 1.33 by HEMS and 1.25 ± 0.75 by dye during surgery, but no SLNs were detected as transcutaneous shining fluorescent spots on the TV monitor.

DISCUSSION

Current SLN detection methods, such as radioisotopes and blue dyes, show good results, and considerable evidence regarding the SLN biopsy concept supports its application to many types of cancer.[8,10,11,20] In SLN biopsy, a false-negative is the worst error, but SLNs are sometimes not identified, because both methods have some drawbacks.

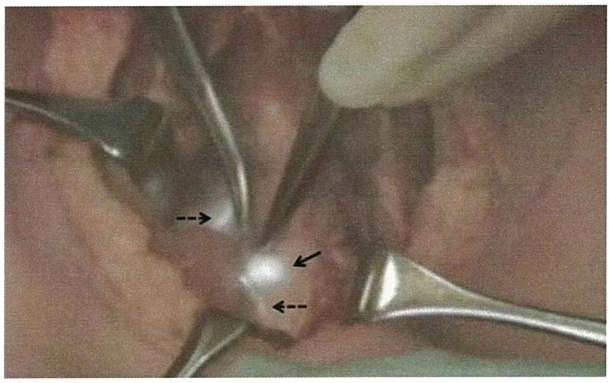

FIG. 5 Color image of intraoperative real-time lymphography showing the lymphatic vessel (*dotted arrows*) and the SLN (*arrow*)

Radioisotopes have a "shine-through phenomenon".[21] When the primary lesion is directly injected with radioactive tracer, its radioactivity is so strong that the radioactivity of true SLNs is masked, especially SLNs of head and neck cancer that are located close to the primary lesion. This problem sometimes makes it difficult to identify the SLNs. Blue dye also has disadvantages, because SLNs cannot be identified transcutaneously, and sometimes drainage needed for sufficient staining does not occur.[13]

If these drawbacks were to be overcome, it would be possible to identify and harvest SLNs in an accurate, safe, fast, and reliable manner. We hypothesized that HEMS could be a promising device for overcoming these drawbacks. The purpose of this study was to test the feasibility of head and neck SLN biopsy using HEMS and to compare it to the blue dye method.

ICG fluorescence detection can allow transcutaneous visualization of SLNs.[10] HEMS detected all SLNs in rabbits transcutaneously, but those of pigs were not identified. Because near-infrared (NIR) fluorescence cannot penetrate thick tissues, a color CCD camera does not visualize NIR fluorescence from a deep SLN embedded in the deep fatty tissue. The pig tissues were thicker than those from the rabbits (4 cm vs. 1 cm).

Kitai et al. reported that NIR fluorescence was observed from an ICG solution embedded 1 cm deep in a material with optical properties comparable to human tissue in a preliminary study that used a phantom.[15] Ishikawa et al. also reported that NIR using endoscopy can penetrate fatty tissues up to a depth of only 3 mm.[22] From this perspective, HEMS, which can penetrate up to 1.5–2.0 cm, is superior to other near-infrared camera systems (data not shown).

HEMS captures ICG fluorescence images on a color CCD camera. The major difference between HEMS and other NIR fluorescence-using devices is that HEMS can visualize ICG-enhanced structures against a vividly colored background. We can obtain better visualization to

detect SLNs, and it allows transcutaneous real-time lymphography for intraoperative identification of SLNs. Color TV monitor images are better and quicker than monochrome images for finding SLNs.

Using HEMS, the mean ± SD number of SLNs was 1.75 ± 1.33 in pigs and 1.25 ± 0.75 in rabbits. Using blue dye, the mean ± SD number was 1.25 ± 0.5 in pigs and 1 ± 0 in rabbits. HEMS detected all SLNs stained by the blue-dye method. This study showed that HEMS increased the SLN detection rate and decreased the false-negative rate. The accuracy of HEMS was due to an increased number of analyzed SLNs, because SLNs did not stain green after injection of less than 20 mg of ICG, although they showed a bright fluorescence signal.[13]

In this study, HEMS as an ICG fluorescence imaging detection method could not be compared against radioisotope methods because of our institution's animal regulations. Hirche et al. reported that the ICG fluorescence imaging detection rate was 83%, and that of a combination of radioisotope and blue dye was 75% in anal cancer.[14] Hojo et al. reported that the ICG fluorescence imaging detection rate was 99.3%, with 92.9% for blue dye and 100% for radioisotope.[23] Because there is a risk of missing appropriate SLNs when using only one method, ICG fluorescence would be a promising method if it were combined with the radioisotope method.

HEMS also has disadvantages; ICG fluorescence is a time-limited method, with a maximum duration of 4 h after injection without loss of fluorescence, and the operating room must be dimmed to improve camera sensitivity.

SLN detection using HEMS is feasible, with success comparable to the blue dye method. However, the use of HEMS is limited by skin thickness and the possible deep location of SLNs; therefore, new maneuvers are needed for transcutaneous imaging, such as direct manual compression of the surface tissues and air insufflation of the pharynx. HEMS could be combined with radioisotope methods in obese patients as the first step. The results described in this report justify a clinical trial on the feasibility of HEMS in humans.

In the future, HEMS could lead to important improvements in the treatment of cancer if it is found to improve the ability to detect SLNs transcutaneously under varied conditions.

CONCLUSIONS

This report presented the feasibility of the new SLN method in animal models. ICG fluorescence using HEMS may offer many advantages over current methods, and it warrants further study leading to human clinical trials.

ACKNOWLEDGMENT This study was supported by a Health and Labour Sciences Research Grant for Clinical Cancer Research (H21-Gannorinshou-Ippan-016) from the Ministry of Health, Labour and Welfare, Japan.

DISCLOSURE None.

REFERENCES

1. Shah JP, Candela FC, Poddar AK. The patterns of cervical lymph node metastases from squamous carcinoma of the oral cavity. *Cancer.* 1990;66(1):109–13.
2. Morton DL, Thompson JF, Cochran AJ, et al. Sentinel-node biopsy or nodal observation in melanoma. *N Engl J Med.* 2006; 355(13):1307–17.
3. Riber-Hansen R, Nyengaard JR, Hamilton-Dutoit SJ, Steiniche T. Stage migration after minor changes in histologic estimation of tumor burden in sentinel lymph nodes: the protocol trap. *Cancer.* 2009;115(10):2177–87.
4. Shoaib T, Soutar DS, Prosser JE, et al. A suggested method for sentinel node biopsy in squamous cell carcinoma of the head and neck. *Head Neck.* 1999;21(8):728–33.
5. Kohno N, Ohno Y, Kihara K, et al. Feasibility of sentinel lymph node radiolocalization in neck node-negative oral squamous cell carcinoma patients. *ORL J Otorhinolaryngol Relat Spec.* 2003; 65(1):66–70.
6. Kontio R, Leivo I, Leppanen E, Atula T. Sentinel lymph node biopsy in oral cavity squamous cell carcinoma without clinically evident metastasis. *Head Neck.* 2004;26(1):16–21.
7. Ross GL, Soutar DS, Gordon MacDonald D, et al. Sentinel node biopsy in head and neck cancer: preliminary results of a multicenter trial. *Ann Surg Oncol.* 2004;11(7):690–6.
8. Veronesi U, Paganelli G, Viale G, et al. A randomized comparison of sentinel-node biopsy with routine axillary dissection in breast cancer. *N Engl J Med.* 2003;349(6):546–53.
9. Tafra L, Lannin DR, Swanson MS, et al. Multicenter trial of sentinel node biopsy for breast cancer using both technetium sulfur colloid and isosulfan blue dye. *Ann Surg.* 2001;233(1): 51–9.
10. Tajima Y, Murakami M, Yamazaki K, et al. Sentinel node mapping guided by indocyanine green fluorescence imaging during laparoscopic surgery in gastric cancer. *Ann Surg Oncol.* 2010;17(7):1787–93.
11. Kell MR, Kerin MJ. Sentinel lymph node biopsy. *BMJ.* 2004;328(7452):1330–1.
12. Handa T, Katare RG, Nishimori H, et al. New device for intraoperative graft assessment: HyperEye charge-coupled device camera system. *Gen Thorac Cardiovasc Surg.* 2010;58(2):68–77.
13. Hirche C, Murawa D, Mohr Z, Kneif S, Hunerbein M. ICG fluorescence-guided sentinel node biopsy for axillary nodal staging in breast cancer. *Breast Cancer Res Treat.* 2010;121(2): 373–8.
14. Hirche C, Dresel S, Krempien R, Hunerbein M. Sentinel node biopsy by indocyanine green retention fluorescence detection for inguinal lymph node staging of anal cancer: preliminary experience. *Ann Surg Oncol.* 2010;17(9):2357–62.
15. Kitai T, Inomoto T, Miwa M, Shikayama T. Fluorescence navigation with indocyanine green for detecting sentinel lymph nodes in breast cancer. *Breast Cancer.* 2005;12(3):211–5.
16. Pitman KT, Sisk JD. Endoscopic sentinel lymph node biopsy in a porcine model. *Laryngoscope.* 2006;116(5):804–8.
17. Curry JM, Bloedon E, Malloy KM, et al. Ultrasound-guided contrast-enhanced sentinel node biopsy of the head and neck in a porcine model. *Otolaryngol Head Neck Surg.* 2007;137(5):735–41.

18. Malloy KM, Cognetti DM, Wildemore BM, et al. Feasibility of endoscopic sentinel node biopsy in the porcine neck. *Otolaryngol Head Neck Surg.* 2007;136(5):806–10.
19. Tagaya N, Yamazaki R, Nakagawa A, et al. Intraoperative identification of sentinel lymph nodes by near-infrared fluorescence imaging in patients with breast cancer. *Am J Surg.* 2008;195(6):850–3.
20. Noura S, Ohue M, Seki Y, et al. Feasibility of a lateral region sentinel node biopsy of lower rectal cancer guided by indocyanine green using a near-infrared camera system. *Ann Surg Oncol.* 2010;17(1):144–51.
21. Hayashi T, Furukawa H, Tsutsumida A, Yoshida T. A false-negative sentinel lymph node in the parotid gland of a melanoma patient: a new algorithm for SLN biopsy in the parotid gland. *Int J Clin Oncol.* 2010;15(5):504–7.
22. Ishikawa K, Yasuda K, Shiromizu A, Etoh T, Shiraishi N, Kitano S. Laparoscopic sentinel node navigation achieved by infrared ray electronic endoscopy system in patients with gastric cancer. *Surg Endosc.* 2007;21(7):1131–4.
23. Hojo T, Nagao T, Kikuyama M, Akashi S, Kinoshita T. Evaluation of sentinel node biopsy by combined fluorescent and dye method and lymph flow for breast cancer. *Breast.* 2010;19(3):210–3.

Donepezil, Anti-Alzheimer's Disease Drug, Prevents Cardiac Rupture during Acute Phase of Myocardial Infarction in Mice

Mikihiko Arikawa[1]*, Yoshihiko Kakinuma[1], Takemi Handa[1], Fumiyasu Yamasaki[2], Takayuki Sato[1]

1 Department of Cardiovascular Control, Kochi Medical School, Nankoku, Kochi, Japan, **2** Department of Clinical Laboratory, Kochi Medical School, Nankoku, Kochi, Japan

Abstract

Background: We have previously demonstrated that the chronic intervention in the cholinergic system by donepezil, an acetylcholinesterase inhibitor, plays a beneficial role in suppressing long-term cardiac remodeling after myocardial infarction (MI). In comparison with such a chronic effect, however, the acute effect of donepezil during an acute phase of MI remains unclear. Noticing recent findings of a cholinergic mechanism for anti-inflammatory actions, we tested the hypothesis that donepezil attenuates an acute inflammatory tissue injury following MI.

Methods and Results: In isolated and activated macrophages, donepezil significantly reduced intra- and extracellular matrix metalloproteinase-9 (MMP-9). In mice with MI, despite the comparable values of heart rate and blood pressure, the donepezil-treated group showed a significantly lower incidence of cardiac rupture than the untreated group during the acute phase of MI. Immunohistochemistry revealed that MMP-9 was localized at the infarct area where a large number of inflammatory cells including macrophages infiltrated, and the expression and the enzymatic activity of MMP-9 at the left ventricular infarct area was significantly reduced in the donepezil-treated group.

Conclusion: The present study suggests that donepezil inhibits the MMP-9-related acute inflammatory tissue injury in the infarcted myocardium, thereby reduces the risk of left ventricular free wall rupture during the acute phase of MI.

Citation: Arikawa M, Kakinuma Y, Handa T, Yamasaki F, Sato T (2011) Donepezil, Anti-Alzheimer's Disease Drug, Prevents Cardiac Rupture during Acute Phase of Myocardial Infarction in Mice. PLoS ONE 6(7): e20629. doi:10.1371/journal.pone.0020629

Editor: Markus M. Heimesaat, Charité, Campus Benjamin Franklin, Germany

Received January 27, 2011; **Accepted** May 6, 2011; **Published** July 5, 2011

Funding: This work was supported by a Grant-in-Aid for Young Scientists (21790729) from Japan Society for the Promotion of Science. The funders had no role in study design, data collection and analysis, decision to publish, or preparation of the manuscript.

Competing Interests: The authors have declared that no competing interests exist.

* E-mail: marikawa@kochi-u.ac.jp

Introduction

In 2000, K. J. Tracey and coworkers reported the role of efferent vagus nerve signaling in modulating inflammation [1]. The electrical stimulation of the efferent vagus nerve releases acetylcholine (ACh), a principal vagal neurotransmitter, and ACh seems to attenuate systemic inflammatory responses by inhibiting the production of pro-inflammatory cytokines from activated macrophages and other immune cells. The 'cholinergic' anti-inflammatory pathway would provide a new therapeutic modality for the clinical treatment of inflammatory disorders [2].

We have reported another aspect of the beneficial effect of the vagal nerve stimulation [3]. Chronic vagal nerve stimulation with an implantable stimulator prevented the cardiac pumping dysfunction and improved long-term survival in rats with chronic heart failure after large myocardial infarction (MI). Although the precise mechanisms of the protective effect of the vagal nerve stimulation on cardiomyocytes have not yet been fully elucidated, our previous studies have clearly demonstrated that the antiarrhythmogenic effects are mediated by preservation of the gap-junctional protein, connexin 43, and the antiapoptotic effects are derived from the PI3K/Akt/HIF-1α signaling pathway in cardiomyocytes, both of which are proposed to be involved in the mechanism of the cardioprotective effect of the vagal nerve stimulation [4,5]. The therapeutic modality of the vagal nerve stimulation has been recently applied for patients with heart failure in a clinical trial without significant side effects [6–8], however, it might have disadvantages because it is an invasive procedure suffering a surgical strain to the patients. Since a novel and a more effective therapeutic strategy against heart failure is mandatory, we have studied the effect of an acetylcholinesterase inhibitor, donepezil, on heart failure expecting the cardioprotective effect. Donepezil is a therapeutic acetylcholinesterase inhibitor for treatment of Alzheimer's disease, a neurodegenerative disorder characterized with a depletion of nicotinic ACh receptors and a loss of cholinergic neurons [9]. A number of studies using animal models have demonstrated that donepezil possesses the neuroprotective activity *in vivo* [10], and *in vitro* [11,12]. In addition, it has been recently demonstrated that the administration of donepezil reproduced the effect of the vagal nerve stimulation. For example, donepezil has been shown to 1) prevent cardiac remodeling with enhancing vagal activity in a rat chronic MI model [13], 2) improve survival by preventing pumping failure in a mouse volume overload model [14] and 3) up-regulate angiogenesis by modulating angiogenesis-responsible machinery of endothelial

cells in a mouse ischemic hindlimb model [15], indicating that the donepezil possesses not only neuroprotective but cardioprotective effects. In comparison with such chronic effects, however, the acute effect of donepezil during an acute phase of MI remains unclear.

Even though surgical techniques for ischemic heart failure have been improved, left ventricular free wall rupture has been still one of the most lethal complications occurring in up to 10% patients with acute MI [16]. Clinical and pathological studies in humans have reported that the mean interval between diagnosis of acute MI and the appearance of left ventricular free wall rupture ranged from 1 to 5 days after MI [17–21]. Approximately 60% of the left ventricular free wall rupture occurred within 5 days postinfarction [22]. A large number of studies have shown that a severe inflammatory cell infiltration following acute MI markedly activates various matrix metalloproteinases (MMPs) which rapidly degrade the fibrillar collagen network and weaken the tensile strength of the infarcted myocardium, resulted in wall rupture [23,24]. Therefore, the suppression of MMPs during an acute phase of MI is a potential target for the therapeutic intervention [25–30].

In the present study, noticing recent findings of a cholinergic mechanism for anti-inflammatory actions, the effect of donepezil on inflammatory response and cardiac rupture during the acute phase of MI was investigated. Present results showed that donepezil inhibits MMP-9, a member of the MMP family, in macrophages and attenuates infiltration of inflammatory cells into the infarcted myocardium, thereby reduces the risk of cardiac rupture during the acute phase of MI, suggesting that donepezil can be a new potential candidate for a clinically useful drug for heart failure therapy.

Materials and Methods

Animals

Male C57BL/6 mice (Japan SLC inc., Hamamatsu, Japan) aged between 9 and 11 weeks and weighed 20–25 g were used. All animal procedures were performed in strict accordance with guidelines of the Physiological Society of Japan and were approved by the Animal Research Committee of Kochi Medical School (Permit Number: C-00036).

Macrophage isolation and sample preparation

From mice euthanized with ether inhalation, peritoneal macrophages were obtained by washing out the abdominal cavity with ice-cold phosphate buffered saline (PBS). Cells were collected by centrifugation, resuspended in RPMI 1640 medium (Sigma-Aldrich Japan, Tokyo, Japan) containing 10% fetal bovine serum (Tissue Culture Biologicals, CA, USA), and seeded at a concentration of more than 3×10^6 cells/well of a 12-well plastic dish. After incubation at 37°C for 2 hrs, non-adherent cells were flushed away and adhered cells were further incubated at 37°C for 18 hrs in RPMI 1640 medium with or without donepezil, an acetylcholinesterase inhibitor, provided by Eisai Co., Ltd. (Tokyo, Japan) at a concentration of 100 μM. Three hours after the addition of lipopolysaccaride (LPS, Sigma-Aldrich Japan, Tokyo, Japan) at a concentration of 10 ng/ml, culture medium was collected from each well and mixed with same amount of twice concentrated sample buffer (125 mM Tris-HCl (pH 6.8), 20% glycerol, 4% sodium dodecyl sulfate (SDS), 10% 2-mercaptoethanol and 0.1% bromophenol blue), or the sample buffer was directly added to the adhered cells. Protein samples were boiled with a THERMO BLOCK ND-M11 (Nissin, Tokyo, Japan) for 5 min before electrophoresis.

Immunocytochemistry

Isolated macrophages seeded onto a glass-bottom dish (Matsunami Glass Industry, Ltd., Tokyo, Japan) were stimulated by LPS with or without donepezil pretreatment as described above. Cells fixed with 4% paraformaldehyde phosphate buffer solution for 30 min at room temperature were permeabilized with 1% buffered triton X-100 for 15 min, and blocked with 10% goat serum in tris buffered saline with 0.2% Tween 20 (TBS-T) for 30 min. Thereafter, cells were incubated with a rabbit polyclonal anti mouse matrix metalloproteinase-9 (MMP-9) antibody (Abcam, Tokyo, Japan) diluted 1:500 for 60 min and a fluorescent conjugated goat anti rabbit IgG antibody (Invitrogen, Tokyo, Japan) diluted 1:1000 for 45 min at room temperature. After nuclei were counterstained with Hoechst 33258 (Invitrogen, Tokyo, Japan), fluorescence was visualized and photographed with a confocal laser scanning microscope FV-300 with a fluoview software version 4.3 (Olympus, Tokyo, Japan).

Animal model and drug administration

After induction of anesthesia by intraperitoneal injection of pentobarbital (50 mg/kg), mice were put on a heated pad and artificially ventilated (5% carbon dioxide and 95% oxygen) with a volume-controlled MiniVent Model 845 Ventilator for mice (Harvard Apparatus, MA, USA) with a stroke volume of 300 μL and a respiratory rate of 130 breaths/min. Under a surgical microscope (Leica M6541, Leica Microsystems, Tokyo, Japan), a left-side thoracotomy was performed and a pericardium was partially stripped to expose the heart. The left anterior descending coronary artery was ligated with an 8-0 silk suture (Akiyama MEDICAL MFG, Tokyo, Japan). Myocardial ischemia was confirmed by blanching of the anterior wall of the left ventricle and ST segment elevation on the electrocardiogram. In sham-operated mice, the same surgical procedures were performed except for the ligation of the coronary artery. After the chest was closed with a 5-0 polyester suture (Bear Medic, Tokyo, Japan), animals were kept warm under a heat lamp during the recovery period. Infarcted mice were randomly divided into untreated and donepezil-treated groups. Donepezil was administrated orally at dosage of 5.0 mg/kg/day. Mice recovered from the surgical damage were housed under identical conditions within 6 hrs after surgery and given food and water or drug *ad libitum*. The cages were inspected daily for morbidity and mortality, and autopsy was immediately performed to determine the cause of death in all dead animals. Cardiac rupture was confirmed based on a diagnosis of the presence of a large amount of blood clot within the chest cavity or the wall perforation at the left ventricular infarct area, and a rupture rate was calculated in percentage as a number of ruptured animals divided by a number of total operated animals in each group.

Heart rate and blood pressure measurement

At 3 days after surgery, sham-operated and infarcted mice were kept in a preheated dark chamber for at least 10 min in order to increase blood flow to the tail. The mouse tail was inserted through an appropriate cuff, and heart rate (HR) and systolic blood pressure (SBP) were measured noninvasively by a computer-automated tail-cuff system with a data analysis software (BP-98A, Softron, Tokyo, Japan) according to the manufacturer's instructions. HR and SBP were finally determined by averaging the data obtained from 5 to 10 successful measurement cycles.

Histology and immunohistochemistry

Mice were anesthetized and sacrificed at appropriate time points after surgery. Hearts were immediately excised and washed with ice-cold PBS. Paraformaldehyde-fixed and paraffin-embedded heart samples were sectioned transversely at 3–5 μm thick at a middle part of the left ventricular infarct area. After dewaxed and rehydrated by sequential treatment with xylene and a graded ethanol series, sections were routinely stained with hematoxylin and eosin (HE) or Masson's trichrome staining. Histological images were captured with a digital camera and wall thickness was measured. Infarct size was calculated in percentage as total infarct circumference divided by total LV circumference according to the method of Pfeffer [31,32]. Under high power field magnification (×400), the number of nuclei at the border zone of the infarct was manually counted from randomly selected areas (4 areas/section), and expressed as nuclei per square millimeter. For immunohistochemistry, deparaffinized and rehydrated sections were heated at 95°C for 30 min in a Tris-EDTA buffer (Target Retrieval Solution, pH 9, DakoCytomation, Denmark) for antigen retrieval. After a 45 min blocking step with 10% goat serum in TBS-T, sections were incubated with a rabbit polyclonal anti mouse MMP-9 antibody (Abcam, Tokyo, Japan) diluted 1:100 for 90 min and a fluorescent conjugated goat anti rabbit IgG antibody (Invitrogen, Tokyo, Japan) diluted 1:500 for 45 min at room temperature. Sections were counterstained for nuclei with Hoechst 33258 (Invitrogen, Tokyo, Japan). Observations were made with a confocal laser scanning microscope FV-300 (Olympus, Tokyo, Japan).

RT-PCR

From excised hearts, right ventricle and left ventricle including septum were dissected. The left ventricle of the infarcted heart was further separated into infarct and non-infarct area. Infarct tissues were frozen with liquid nitrogen and stored at −80°C until use. Total RNA was isolated from tissues by phenol/chloroform extraction method using TRIzol Reagent (Invitrogen Japan, Tokyo, Japan) according to the manufacturer's instructions. The Reverse Transcriptase XL for RT-PCR kit (Takara, Japan) was used to obtain first-strand cDNA, which was then amplified with gene specific primers by a PCR thermal cycler (TP-600, Takara, Japan). For mouse MMP-9, a sense primer (5′-GCATACTTG-TACCGCTATGG-3′) and an antisense primer (5′-TAACCG-GAGGTGCAAACTGG-3′) were used. Products were electrophoretically fractionated on 2% agarose gels and photographed by Kodak Gel Logic 100 Imaging System and Kodak Molecular Imaging Software v. 4. 5. 0.

Electrophoresis and immunoblotting

The left ventricular infarct area was carefully dissected from an excised heart under a surgical microscope and homogenized in an extraction buffer containing 50 mM Tris-HCl (pH 6.8), 150 mM NaCl, 1% Triton X-100 and 10% SDS. After centrifugation, the supernatants were mixed with same amount of twice concentrated sample buffer and boiled for 5 min. Protein samples obtained from *in vivo* and *in vitro* studies were separated by SDS-polyacrylamide gel electrophoresis (SDS-PAGE) according to the method of Laemmli [33]. For immunoblotting analysis, proteins were electrophoretically transferred to a PVDF-membrane (Immobilon-P, Millipore Japan, Tokyo, Japan) and blocked in a blocking buffer containing 5% dehydrated skim milk (Difco Laboratories Inc., MI, USA) for at least 30 min at room temperature or overnight at 4°C. The membrane was incubated with a rabbit anti mouse MMP-9 antibody (Abcam, Tokyo, Japan) diluted 1:2000 for 90 min, followed by incubation with a horseradish peroxidase (HRP)-conjugated goat anti rabbit IgG antibody (Invitrogen, Tokyo, Japan) diluted 1:5000 for 45 min at room temperature. HRP activity was detected by chemiluminescence using an ECL plus Western Blotting Detection System (GE Healthcare Japan Corporation, Tokyo, Japan).

Gelatin zymography

The enzymatic activity of MMP-9 was measured by gelatin zymography under nonreducing conditions according to the standard procedures. Briefly, macrophage culture media or tissue lysate of left ventricular infarct area were mixed with same amount of twice concentrated sample buffer which does not contain 2-mercaptoethanol, and stored at 4°C for overnight without boiling. The samples were then electrophoretically separated on a polyacrylamide gel containing 1 mg/ml gelatin as a substrate. The gel was washed with 2.5% Triton X-100 solution for 60 min at room temperature, and then incubated with a developing buffer containing 50 mM Tris-HCl (pH 7.5), 200 mM NaCl, 10 mM $CaCl_2$, 1 μM $ZnCl_2$ and 0.02% NaN_3 for 20 hrs at 37°C. The gel was stained with 0.5% Coomassie Brilliant Blue R-250 for 30 min and destained for appropriate time until clear bands were visualized, and was scanned by a digital scanner (ES-2000, Epson Co., Tokyo, Japan).

Statistical analysis

Data are presented either as means ± SD or a percentage compared with a control. Nonparametric comparisons between two groups were performed with a Mann-Whitney U-test. Multiple comparisons among groups were performed with a nonparametric one-way ANOVA using a Kruskal-Wallis test. The mortality data were analyzed by a Chi-square test. A value of $P<0.05$ was considered statistically significant.

Results

Effect of donepezil on macrophage MMP-9

Compared to the control (control, 100.00±7.08%, n = 11), lipopolysaccaride (LPS) treatment at a concentration of 10 ng/ml for 3 hrs significantly increased macrophage matrix metalloproteinase-9 (MMP-9) secretion to culture medium (LPS, 116.16± 5.37% versus control, n = 11, $P<0.01$). However, MMP-9 in culture medium of the donepezil-pretreated macrophages was significantly lower than the control (DPZ/LPS, 76.90±10.92% versus control, n = 11, $P<0.01$). Consequently, donepezil pretreatment reduced the LPS-induced MMP-9 secretion from macrophages by 33.80% ($P<0.01$, Figure 1). In this study, we used donepezil expecting its inhibitory action on acetylcholinesterase. Therefore, the effect of ACh on macrophage MMP-9 was also investigated. However, unexpectedly, the LPS-induced increase of MMP-9 was not inhibited by pretreatment of ACh (100 μM) (ACh/LPS in Figure 2a). Moreover, the MMP-9 inhibition by donepezil was observed even in the presence of a muscarinic ACh receptor blocker, atropine (100 μM) or a nicotinic ACh receptor blocker, mecamylamine (5 μM) (Atr/DPZ/LPS and Mec/DPZ/LPS in Figure 2b). These results indicate that the inhibitory effect of donepezil on macrophage MMP-9 is independent of ACh. The alteration of MMP-9 content within cells before and after LPS treatment with or without donepezil pretreatment was examined (Figure 3a). In the control (control), MMP-9 was stored within cells and also secreted to culture medium (cell, 52.5±4.7 in a.u., n = 6 and medium, 48.5±15.5 in a.u., n = 6). When cells were treated with LPS for 3 hrs (LPS), MMP-9 was significantly decreased in cells (23.6±3.8 in a.u., n = 6, $P<0.01$ versus control) and increased